Applied Catalysis B: Environmental 148–149 (2014) 366–376

Contents lists available at ScienceDirect

Applied Catalysis B: Environmental

journal homepage: www.elsevier.com/locate/apcatb

# Salt-templated synthesis of Ce/Al catalysts supported on mesoporous silica for acetone oxidation

Liang-Yi Lin, Hsunling Bai*

*Institute of Environmental Engineering, National Chiao Tung University, Hsinchu 300, Taiwan*

ARTICLE INFO

*Article history:*
Received 5 June 2013
Received in revised form 10 October 2013
Accepted 15 November 2013
Available online 22 November 2013

*Keywords:*
Aerosol
Mesoporous
Bimetallic
Catalytic oxidation
Acetone

ABSTRACT

A series of bimetallic Ce/Al catalysts supported on mesoporous silica catalysts were prepared through fast salt-templated aerosol process in this study. The source of sodium silicate precursor was from the alkali-extraction of the opto-electronic industrial waste. The inorganic salt formed during the silicate acidification process was served as an effective and low-cost template, which could be simply removed by water washing at room temperature. The Ce/Al-$SiO_2$ catalysts were fabricated under various aerosol-spraying temperatures, and the temperature effects on the structural and surface properties were investigated by XRD, nitrogen physisorption measurement, SEM/TEM, ICP-MS, $^{27}$Al MAS-NMR, UV–vis spectra, $H_2$-TPR and $NH_3$-TPD analyses. The catalytic behavior was further evaluated in terms of acetone oxidation. The results revealed that the catalytic oxidation of acetone is mainly governed by the surface redox property, along with the acidity of the catalysts. The Ce/Al-$SiO_2$-300, with high surface acidity and strong surface reducibility, appeared to have the best acetone catalytic performance at temperatures of 100–300 °C and its $T_{90}$ was at 165 °C under acetone inlet concentration of 1000 ppmv and GHSV of 15,000 $h^{-1}$. Furthermore, compared with literature data which catalysts were prepared using commercial silicon source and traditional organic surfactant templates, Ce/Al-$SiO_2$-300 showed a comparable catalytic performance, indicating the great potential application of Ce/Al-$SiO_2$ catalysts for the catalytic oxidation of acetone.



## 1. Introduction

Catalytic oxidation is one of the attractive technologies for reducing volatile organic compounds (VOCs) emission as it can take place at lower working temperatures than those required for thermal oxidation treatment, which benefits in lowering the energy consumption and reducing the operating costs [1,2]. Supported noble metals are most widely studied catalysts for VOC oxidation; however, their high prices significantly restrict their applications [3–6]. Recently, supported metal oxides (Cu, Mn, Ce, Fe, Ti, etc.) have been proposed as promising alternatives to noble metals for VOC oxidation processes because of their relatively low cost and high catalytic activity [7–10]. Among them, supported cerium oxide ($CeO_2$) has been demonstrated to be effective for VOCs abatement, attributed to its high oxygen storage capacity and easy release of active oxygen species via facile $Ce^{3+}/Ce^{4+}$ redox cycle [11–15].

In the preparation of supported catalysts, the selection of a suitable support and/or preparation method are of great importance to obtain catalysts with high activity, since the nature of the support has a great impact on the formed active phase (e.g. oxidation state and metallic dispersion), which are all crucial parameters for their catalytic behavior [16–19]. Mesoporous silicas with high surface area and uniform mesochannels have gained considerable interest as catalyst supports for the synthesis of uniform and well-dispersed metal/metal oxide nanoparticles via their hosting into the silica matrix [20–23]. In recent years, various mesoporous metal-$SiO_2$ materials have been prepared via direct hydrothermal method or postsynthesis wet impregnation and their catalytic performance for VOCs removal have been explored [24–31]. Mu et al. [32] depicted that the application of direct hydrothermal method favored the formation of $CeO_2$ nanoparticles on SBA-15 with higher surface area and better dispersion than traditional impregnation method, which easily resulted in the appearance of bulk $CeO_2$ species, blocking the channels of SBA-15. The formed nanosized $CeO_2$ species on SBA-15 showed easier reduction of surface oxygen species than that of bulk species, resulting in the enhanced catalytic efficiency of benzene oxidation. Previously, we have explored the rapid synthesis of novel bimetallic Ce/Al-containing hexagonally ordered mesoporous silica particles (Ce/Al-MSP) via an aerosol-assisted self-assembly method for potential applications in catalytic oxidation of acetone [33]. The Ce/Al-MSP exhibited higher catalytic activity than that of

* Corresponding author at: Institute of Environmental Engineering, National Chiao Tung University, 1001 University Road, Hsinchu 300, Taiwan.
Tel.: +886 3 5731868; fax: +886 3 5725958.
*E-mail address:* hlbai@mail.nctu.edu.tw (H. Bai).

0926-3373/$ – see front matter © 2013 Elsevier B.V. All rights reserved.
http://dx.doi.org/10.1016/j.apcatb.2013.11.026

Ce/ZSM-5, presumably because of its higher surface area and better metallic dispersion.

The general strategy of the synthesis of mesoporous metal-$SiO_2$ materials involves the use of hard templates (e.g. polystyrene) and/or soft templates (e.g. surfactants) as structure-directing agents, which control the growth of structure and the morphologies of the products [32–39]. In most cases, the pure products were obtained only after the complete removal of the preformed templates by calcination process. However, the requirement of heat treatment (typically > 450 °C) not only is highly energy-consuming, but also would easily result in the extensive growth of larger and aggregated metal particles (poor metallic dispersion) due to the sintering effect, which destroyed the regularity of the mesostructure and decreased metal utilization in catalyzed reactions at the same time [25,40]. In addition, most of the organic templates are expensive, which would pose cost barriers of the application of these catalysts at an industrial level. In this regard, avoiding the use of organic templates to prepare active mesoporous metal-$SiO_2$ composite seems highly desirable. To the authors' knowledge, there is no report available on the synthesis of mesoporous metal-$SiO_2$ materials without adding any organic templates, and also there is no report on demonstrating their potential to serve as catalysts for their catalytic oxidation of VOCs.

For the first time, a series of bimetallic Ce/Al-containing mesoporous silica composites (Ce/Al-$SiO_2$) were synthesized via a salt-templated aerosol method, and investigated for catalytic oxidation of acetone vapors. The inorganic salt of $NaNO_3$, which is in situ formed during the preparation of precursor sols, is employed to replace the traditional organic templates as the templating medium. And the sodium silicate solution, which is extracted from the waste silicate of the opto-electronic industry, is used as the silicon precursor in order to obtain an environmental-friendly and economical synthesis process. The chemical composition of opto-electronic industrial waste silicate is primarily $(NH_4)_2SiF_6$ and $SiO_2$, which makes it a potentially feasible silica source [41,42]. The mesoporous Ce/Al-$SiO_2$ composite with various structural and surface properties were prepared under various aerosol-spraying temperatures, and the structural-performance correlation of the catalysts has been clearly demonstrated in the present work. In addition, the catalytic performance of the obtained Ce/Al-$SiO_2$ is compared to that of Ce/Al-MSP, which was prepared using commercial silicon precursor via traditional surfactant-templated approach.

## 2. Experimental

### 2.1. Synthesis of Ce/Al-$SiO_2$ catalysts

The aerosol fabrication of Ce/Al-$SiO_2$ was carried out in a home-made apparatus depicted in Fig. S1. The sodium silicate solution was prepared by mixing opto-electronic waste powder with 6 M NaOH solution at room temperature for 3 h. Table S1 shows the chemical composition of the raw waste powder and the silicate solution after extraction with NaOH solution. In a typical procedure, 189 ml of waste silicate solution was firstly acidified by adding nitric acid to bring down the pH to 2 with constant stirring. Meanwhile, 0.55 g of aluminum nitrate and 0.32 g of cerium nitrate (dissolved in 20 ml of DI water) was added into the above acidified silicate solution and the combined mixtures were then stirred for 30 min. The molar composition of the precursor mixture was 1 $SiO_2$: 2.59 Na: 0.02 Al: 0.05 Ce: 280 $H_2O$: 2.86 $HNO_3$. The solution was then nebulized by an ultrasonic atomizer (1.8 MHz) with a dry and clean air stream of 2 slpm flow rate and the droplets were passed through a heating zone in which the temperature was controlled at 200, 300, 400 and 500 °C, respectively. After the heating process, the as-prepared samples were collected downstream of the reactor by a high-efficiency filter. Finally, they were recovered by washing and filtration with DI water followed by drying in an oven at 110 °C. The obtained samples prepared under different aerosol-spraying temperatures were denoted as Ce/Al-$SiO_2$-200, Ce/Al-$SiO_2$-300, Ce/Al-$SiO_2$-400 and Ce/Al-$SiO_2$-500. Furthermore, an active silica solution of pH 2 without addition of nitric acid was also prepared using a procedure of cation-exchange resin to produce a reference sample, named as Ce/Al-$SiO_2$-300-NP.

For comparison purpose, the preparation of bimetallic Ce/Al-containing hexagonally ordered mesoporous silica particle (Ce/Al-MSP) was also presented, using sols of commercial tetraethylorthosilicate and cetyltrimethylammonium bromide as the silicon source and mesostructure-directing template, respectively, with similar procedures described in the synthesis of Ce/Al-$SiO_2$ materials. The molar gel composition of the synthesized mixture was 1 $SiO_2$:0.18 CTAB:0.02 Al:0.05 Ce:10 ethanol:80 $H_2O$:0.008 HCl. The as-synthesized Ce/Al-MSP powder was calcined at 550 °C for 6 h in air to remove the residual surfactant. Detailed procedures on the synthesis of Ce/Al-MSP can be referred to Wang and Bai [33,43].

### 2.2. Characterization

The chemical composition of the raw waste powder is determined by energy-dispersive X-ray spectroscopy in a scanning electron microscope (SEM, HITACHI-S4700). The elemental silica, cerium, and aluminum content in the samples were analyzed by an inductively coupled plasma-mass spectrometer (ICP-MS, SCIEX ELAN 5000). Powder X-ray diffraction patterns of samples were recorded by using Rigaku X-ray diffractometer equipped with nickel-filtered Cu Kα (λ = 1.5405 Å) radiation. The diffractograms of the mesoporous samples were recorded in the $2\theta$ range 10–80° in steps of 0.6° with a count time of 60 s at each point. Nitrogen adsorption-desorption isotherm were measured at 77 °K on a Micromeritics ASAP 2020 analyzer. The sample was degassed at 180 °C for 3 h before measurements. Specific surface area was calculated by using the Brunauer–Emmett–Teller (BET) method in the relative pressure range $P/P_0$ = 0.05–0.3. The pore size distribution was obtained from the analysis of the adsorption branch of the isotherm by nonlocal density functional theory (NLDFT) based on the model of spherical cavity [44,45]. Pore volumes were obtained from the volumes of nitrogen adsorbed at $P/P_0$ = 0.95 or in the vicinity. The morphology of the materials was observed via the SEM (HITACHI-S4700) images. TEM images of the samples were observed with a JEOL JEM 1210 TEM instrument operated at 120 keV with the samples (5–10 mg) ultrasonicated in ethanol and dispersed on carbon film supported on copper grids (200 mesh).

$^{27}$Al NMR high speed magic angle spinning (MAS) spectra of the powdered samples were recorded at room temperature on a Bruker DSX 400 WB NMR Spectrometer. The Larmor frequency was 104.1 MHz and aluminum chloride was used as an external reference material. UV–vis spectra of the samples were carried out by using a HITACHI U3010 spectrophotometer equipped with a diffuse reflectance integrating sphere coated with aluminum oxide which served as a reference material. All the samples were recorded in the spectral range between 800 and 200 nm. $H_2$-TPR experiments were performed with an AutoChem II 2920 analyzer. The samples were pretreated in air at 200 °C for 2 h. After that, the experiments were carried out from 50 °C to 700 °C at a heating rate of 10 °C/min in 10% $H_2$/Ar. The $H_2$ consumption was determined by a TCD detector. $NH_3$ temperature-programmed desorption ($NH_3$-TPD) was performed on the same Auto Chem II apparatus. Prior to the $NH_3$-TPD experiments, the samples were preheated in air at 200 °C for 2 h and cooled to 50 °C. Then the samples were exposed to a flow of 15% $NH_3$/He at 50 °C for 1 h, following by Ar purging for 1 h. Finally, the

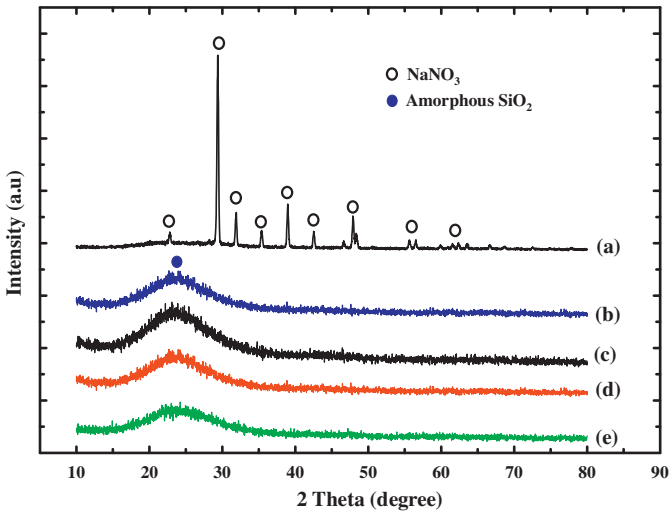


**Fig. 1.** Wide-angle XRD patterns of (a) as-prepared Ce/Al-$SiO_2$-300 and washed Ce/Al-$SiO_2$ prepared with various aerosol-spraying temperatures of (b) 200, (c) 300, (d) 400 and (e) 500.

temperature was raised to 900 °C in an Ar flow at a heating rate of 10 °C/min.

### 2.3. Catalytic abatement of gaseous acetone

Catalytic tests were performed by a vertical and downward flow reactor system. The reactor was made of Pyrex glass tube with 0.8 cm internal diameter. The reactor was heated to the desired temperature with a tubular furnace. Catalysts were tested in 16–30 mesh powdered form and placed in the middle of the glass reactor supported with thin layers of glass wool on both sides. Prior to each catalytic reaction test, the samples were pretreated by heating at 200 °C for 2 h, and then cooled to room temperature. The concentration of acetone was controlled by passing the clean and compressed air through an impinger containing liquid acetone that was kept in a constant temperature-controlled water bath at −10 °C. The total inlet flow rate was controlled to have a GHSV of 15,000 $h^{-1}$ at room temperature (25 °C). Then, reaction temperature was increased stepwise from 100 °C to 300 °C. The inlet and outlet concentrations of acetone were analyzed by a gas chromatograph (GC 7890A, Agilent) equipped with a flame ionization detector (FID). The removal efficiency of acetone was defined by that

$$\text{Removal}\,(\%) = \frac{I - O}{I} \times 100\%,$$

where $I$ and $O$ are the inlet and outlet concentrations of acetone, respectively.

## 3. Results and discussion

### 3.1. Characterization of Ce/Al-$SiO_2$ catalysts

#### 3.1.1. Microstructure

Fig. 1 shows the powder XRD patterns of the as-prepared Ce/Al-$SiO_2$-300 and all washed Ce/Al-$SiO_2$ samples, which were synthesized using sodium silicate supernatant from opto-electronic industrial waste silicate through salt-templated aerosol process. It can be seen that the as-prepared Ce/Al-$SiO_2$-300 sample shows significant diffraction peaks at 2$\theta$ of 23°, 29°, 32°, 35°, 39°, 42°, 48° and 56°, which are indexed on crystalline $NaNO_3$ [46]. To elucidate the above findings, the general theory of acidification of sodium silicate must be addressed. In the preparation of activated silica sols, sodium silicate was acidified and the silica condensation reactions would took place simultaneously to form a siloxane linkage between surface silanol groups, which can be represented as [47]:

$$\text{Si(OH)}_4 + \text{HO—Si(OH)}_3 \rightarrow \text{(OH)}_3\text{Si—O—Si(OH)}_3 + \text{H}_2\text{O} \quad (1)$$

And the reaction of sodium silicate solution acidified with nitric acid during acidification process can be expressed as:

$$\text{Na}_2\text{O}\cdot x\text{SiO}_2 + 2\text{HNO}_3 \rightarrow x\text{SiO}_2\downarrow + 2\text{NaNO}_3 + \text{H}_2\text{O} \quad (2)$$

When the sodium silicate supernatant is acidified by nitric acid, fine crystalline components of $NaNO_3$ are formed. They were further solidified and embedded in silica spheres during spray and heating processes. Since $NaNO_3$ exhibits stronger crystallinity than that of amorphous silica, the sodium salt crystallites are expected to show higher diffraction intensity. Besides, $NaNO_3$ salts are highly soluble so that they can be easily removed by water washing. This is confirmed by XRD results in which a broad diffraction peak at 2$\theta$ of 22° of amorphous silica is observed in all washed Ce/Al-$SiO_2$ samples [48]. It is noteworthy that the trace of the characteristic peaks of crystalline $Al_2O_3$ and $CeO_2$ could not be detected in all washed Ce/Al-$SiO_2$ samples, which suggested the incorporation of Ce and Al species into silica framework or the high surface dispersion of the Ce and Al species have occurred.

#### 3.1.2. Morphology and pore structure

Particle morphology of the washed Ce/Al-$SiO_2$ samples is revealed by the SEM and TEM images. In general, the produced materials show spherical particles as shown in Fig. 2. The TEM images further prove that the washed Ce/Al-$SiO_2$ spheres are porous and they appear to consist of interconnected network. Notably, some fractured and hollow particles were formed in addition to the near spherical particles for the Ce/Al-$SiO_2$-200. The open-broken shell structure probably results from the low degree of nitrate conversion to the oxide which is leached out during water washing. In addition, it can be seen from the HRTEM images that the metal clusters exist between the porous structures of Ce/Al-$SiO_2$ materials, whereas none of them are observed on the external surface of the sphere. This observation may suggest that the metal clusters are well buried within the porous framework of the support.

The pore structures of the Ce/Al-$SiO_2$ materials are analyzed by the nitrogen physisorption measurement, as depicted in Fig. 3(a). All washed samples exhibit type IV isotherms with H2 hysteresis loop, which are indicative of mesoporous materials having networks of interconnected pores [49,50]. The Ce/Al-$SiO_2$-200 sample possesses two-step adsorption isotherm with the first step at $P/P_0$ values in the range of 0.4–0.8, which could be related to the capillary condensation of nitrogen inside nanoporous structure as a result of removal of the salt templates. Secondly, another hysteresis loop lifted up sharply in the $P/P_0$ region of 0.85–0.1, indicating the presence of an additional appreciable amount of larger pores, which could be corresponded to the filling of huge hollow cores, as observed in Fig. 2(a). For Ce/Al-$SiO_2$ sample prepared at temperatures 300–400 °C, a typical single-step adsorption isotherm at a relative pressure of around 0.4–0.8 could be ascribed to the presence of mesopores upon removal of salt templates. Meanwhile, the adsorption capacity and hysteresis loop diminished gradually, which reflected the decrease in the pore volume of the materials. With further increasing the aerosol-spraying temperature to 500 °C, the hysteresis loop shifted slightly in the direction of higher relative pressure with increased adsorption capacity as well as enlarged hysteresis loop, which could be associated with the expansion of the pore width and the pore volume of Ce/Al-$SiO_2$-500.

Fig. 3(b) shows that the pore size distributions, estimated from the NLDFT method, clearly varied with the aerosol-spraying

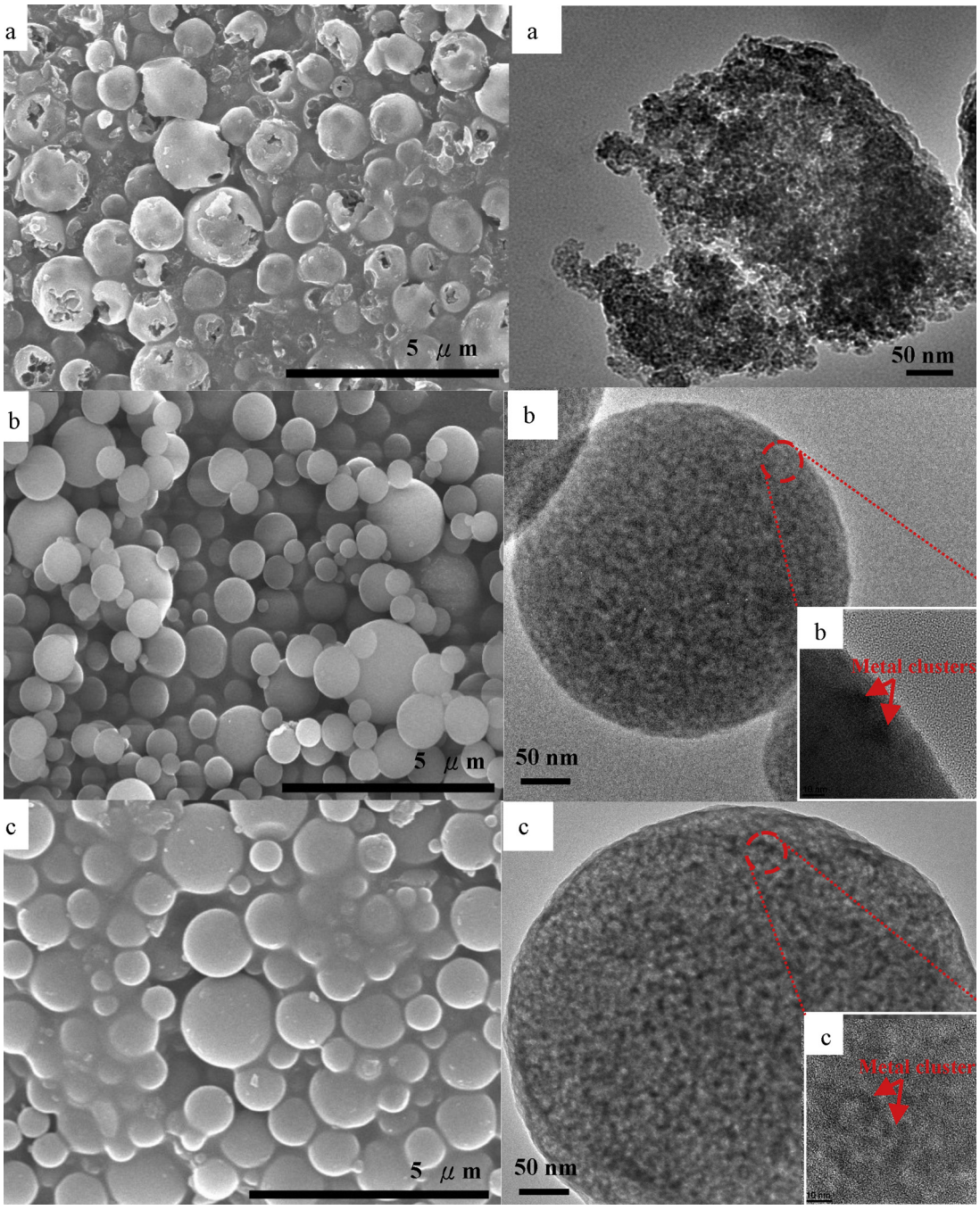


**Fig. 2.** SEM, TEM and HRTEM images of washed (a) Ce/Al-$SiO_2$-200, (b) Ce/Al-$SiO_2$-300 and (c) Ce/Al-$SiO_2$-500 samples.

temperatures. It is well-known that during the quick-drying process of the droplets, the furnace temperature had great influence on the competition between solute diffusion and solvent evaporation, and thus on particle morphology and pore structure [51]. For Ce/Al-$SiO_2$-200, the formation of multi-modal porous particles is obtained, while the large pores at the higher end of the pore diameter might be mainly associated with the formation of hollow-like structures, as observed in Fig. 2(a). Such phenomenon presumably results from nonuniform solute distribution within the droplet and incomplete decomposition of metal nitrates at lower temperature. As the temperature is increased, sample Ce/Al-$SiO_2$-300 with more uniform porous structure is obtained. With further increasing temperatures (400–500 °C), larger salt precipitates are formed during aerosol process, and therefore, the pore diameter would be increased after removal of salt templates. These results imply that the furnace temperature may play a key role in the evolution of particle morphology and pore system of the Ce/Al-$SiO_2$ materials.

The effect of aerosol-spraying temperature on specific surface area ($S_{BET}$) and total pore volume ($V_{pore}$) are summarized in Table 1. It is noted that an increase in surface area with increasing temperature from 200 °C to 400 °C, followed by a drastic decline at higher temperature ($T$ = 500 °C). The increasing surface area with the temperature rise is probably due to the incomplete thermal decomposition of aluminum and/or cerium precipitates that would result in some of aluminum and cerium content being carried away during the washing process and result in less particle surface area. This is further confirmed by thermal gravimetric analysis of

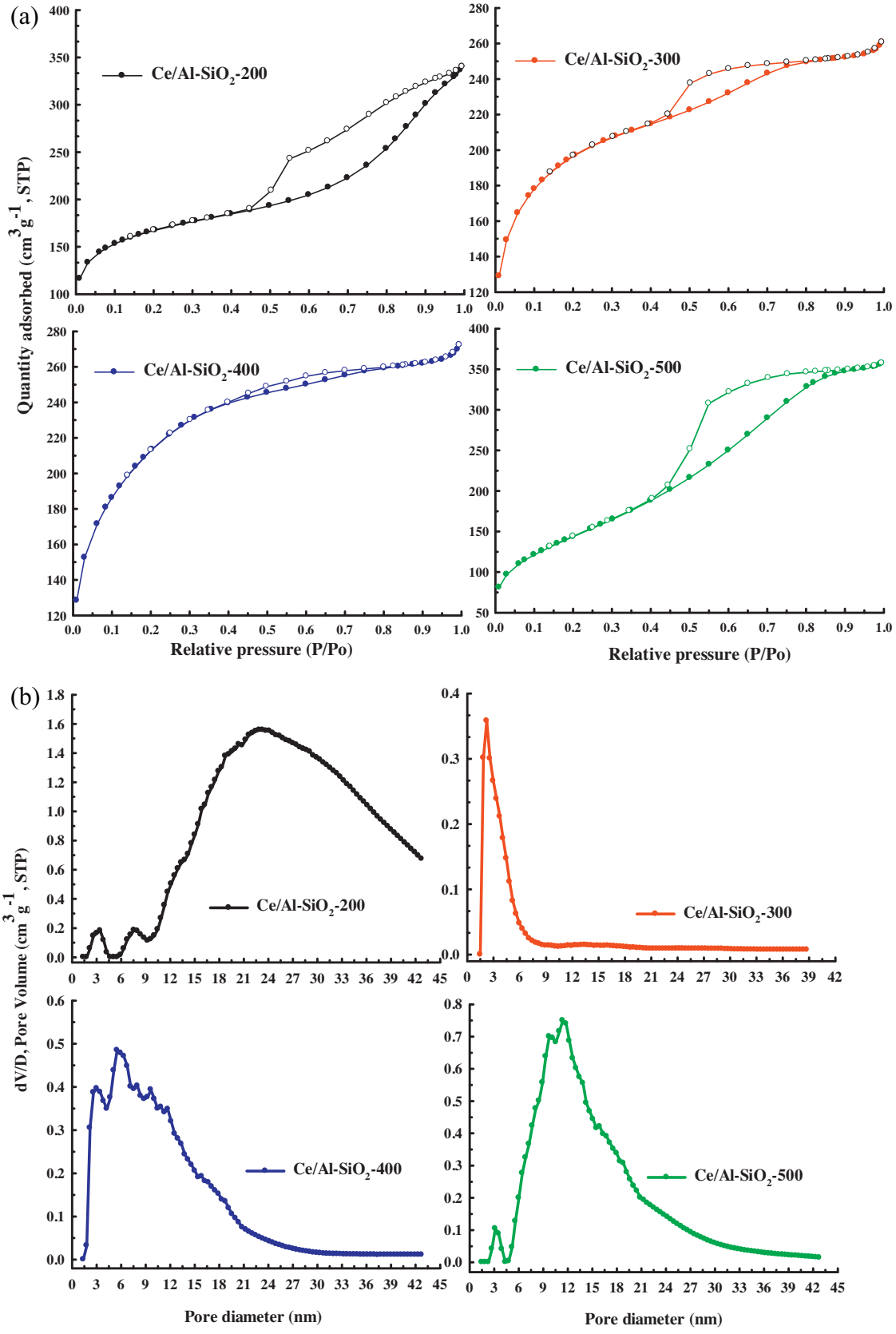


**Fig. 3.** (a) Nitrogen physisorption isotherms and (b) corresponding pore diameter distributions of the washed Ce/Al-$SiO_2$ samples.

**Table 1**
Structural parameters of the washed Ce/Al-$SiO_2$ samples.

| Sample name | $S_{BET}$ ($m^2$/g) | $V_{Pore}$ ($cm^3$/g) | Si (wt%) | Al (wt%) | Ce (wt%) | Na (wt%) | Si/Al molar ratio | Si/Ce molar ratio | Production Yield (%) | Silicon yield (%) |
|---|---|---|---|---|---|---|---|---|---|---|
| Ce/Al-$SiO_2$-300-NP | 8 | 0.005 | 35.1 | 1.30 | 1.80 | 0.33 | 26 | 98 | – | – |
| Ce/Al-$SiO_2$-200 | 581 | 1.01 | 32.4 | 1.23 | 0.30 | 0.41 | 27 | 540 | 47 | 31 |
| Ce/Al-$SiO_2$-300 | 681 | 0.40 | 33.7 | 1.26 | 1.73 | 0.44 | 26 | 97 | 53 | 43 |
| Ce/Al-$SiO_2$-400 | 767 | 0.41 | 34.9 | 1.31 | 2.43 | 0.42 | 26 | 72 | 59 | 47 |
| Ce/Al-$SiO_2$-500 | 522 | 0.55 | 35.7 | 1.43 | 2.99 | 0.40 | 25 | 60 | 60 | 52 |
| Ce/Al-MSP | 917 | 0.71 | 33.1 | 1.2 | 2.7 | – | 27 | 60 | – | – |

aluminum nitrate and cerium nitrate, respectively, as shown in Fig. S2. It is seen that both aluminum nitrate and cerium nitrate show sharp weight losses over the temperature range from 100 °C to 400 °C, and reached a limit of about 14% and 40% weight ratio, respectively, above 400 °C. This clearly implies that the decomposition chemistry is completed at temperatures above 400 °C. Therefore, the aerosol processing of Ce/Al-$SiO_2$ samples at temperatures below 400 °C should produce aluminum and cerium precipitates that have not completely decomposed as indicated by TGA profile. At higher temperature ($T$ = 500 °C), the reducing surface area may be related to the growth of larger crystalline $NaNO_3$ salts. Larger $NaNO_3$ crystallites would lead to a smaller surface area under the same mass basis. Furthermore, Ce/Al-$SiO_2$ samples prepared at intermediate temperatures (300–400 °C) show moderate pore volumes. However, when the temperature is increased, an increase in the overall pore volume is found in Ce/Al-$SiO_2$-500. This is probably associated with extensive growth of larger crystalline $NaNO_3$ salts at 500 °C, resulting in the enlargement of the pore width and pore volume. The increased pore volume of Ce/Al-$SiO_2$-200 presumably arises from the incomplete nitrate decomposition as discussed above, and thus results in the formation of fractured and hollow particles with large pores because of the loss of metal salts during the washing process.

It is well-known that water is encapsulated and mesopore system is created during gel formation in silica [47]. To clarify the role of salts and water on the formation of Ce/Al-$SiO_2$, the washed Ce/Al-$SiO_2$-300-NP sample was prepared from the active silica solution without addition of nitric acid using a procedure of cation exchange. As seen in Fig. S3 and Table 1 that the washed Ce/Al-$SiO_2$-300-NP sample is nonporous material with low specific surface area. The template effect from $NaNO_3$ salts on the physico-chemical properties is further investigated and the results derived from nitrogen physisorption measurement and ICP-MS analyses are summarized in Table S2. Apparently, the as-prepared Ce/Al-$SiO_2$-300 shows high Na contents, low specific surface area and no porosities. After the removal of salt templates by water washing, the surface area and porosities of the Ce/Al-$SiO_2$-300 sample are significantly enhanced, and the 7.30 wt.% Na content in the as-prepared Ce/Al-$SiO_2$-300 sample was reduced to 0.43–0.56 wt.% in the washed Ce/Al-$SiO_2$ samples. Hence the use of 300 ml of water is effective to remove most of the salt templates in the as-synthesized Ce/Al-$SiO_2$-300 sample. Furthermore, Ce/Al-$SiO_2$-200, Ce/Al-$SiO_2$-300, Ce/Al-$SiO_2$-400 and Ce/Al-$SiO_2$-500 samples showed similar sodium contents in the range of 0.40–0.44 wt.% (Table 1). These results clearly demonstrate that the $NaNO_3$ salts, which are in situ formed during the acidification process of sodium silicate, can be employed as effective templates to support the mesostructure, and it can be readily removed by water washing at room temperature.

### 3.1.3. Elemental analysis and coordination environment

The ICP-MS analyses were conducted to determine the metal content in the washed Ce/Al-$SiO_2$ samples prepared at different aerosol-spraying temperatures. As seen in Table 1, similar Al contents were found in all Ce/Al-$SiO_2$ samples, whereas a progressive increase in the Ce content with increasing aerosol processing

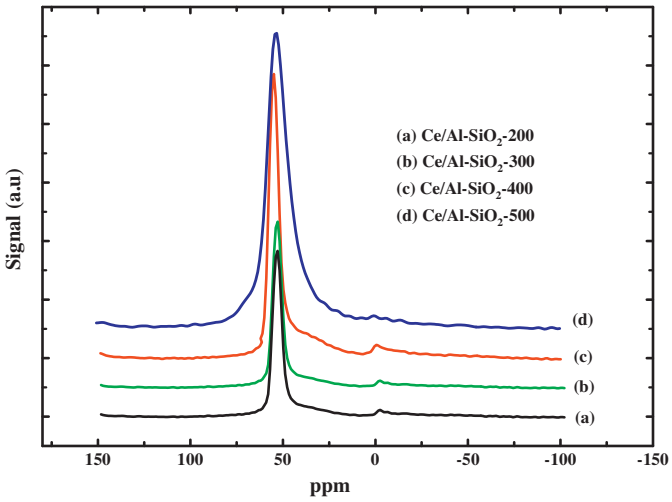


**Fig. 4.** $^{27}$Al MAS-NMR spectra of the washed Ce/Al-$SiO_2$ samples.

temperature was found. This observation is mainly associated with the decomposition behavior of aluminum nitrate and cerium nitrate, respectively, as shown in TGA results (Fig. S2). Thus, one can conclude that the aerosol-spraying temperature had a significant influence not only on the textural properties, but also on the chemical composition of the Ce/Al-$SiO_2$ microspheres.

Solid-state MAS-NMR is a useful tool to investigate the chemical state of the Al species. The Al NMR spectra (Fig. 4) showed that all washed Ce/Al-$SiO_2$ samples exhibit a strong signal at 53 ppm which has been reported to the presence of tetrahedral coordinated Al species [38,52]. In addition, it is noteworthy that a signal at 0 ppm with relatively lower intensity, which corresponded to octahedral coordinated and/or extra-framework Al species, [52] was also observed for all washed Ce/Al-$SiO_2$ samples. The relative intensity indicates that most of Al species are tetrahedral coordinated and incorporated into the framework of the Ce/Al-$SiO_2$ samples.

The UV–vis diffuse reflectance spectra (Fig. 5) are recorded to understand the coordination environment of Ce species in Ce/Al-$SiO_2$ materials. All washed samples exhibit absorption bands with $\lambda_{max}$ at 210–250 and 250–300 nm in the near ultraviolet region from 200 and 400 nm, similar to the results reported for Ce-oxides supported on silica materials [35,52,53]. It has been reported that the former band is attributed to the charge transfer transition of $O^{2-} \rightarrow Ce^{3+}$, whereas the latter band is assigned to that of $O^{2-} \rightarrow Ce^{4+}$ [54]. Hence, the samples might have both $Ce^{3+}$ and $Ce^{4+}$ sites in the silica network. Noticeably, the bands at about 350 nm, which are detected for all Ce/Al-$SiO_2$ samples except Ce/Al-$SiO_2$-200, most probably arise from the presence of polymeric $CeO_2$ cluster species. Moreover, a red shift in the absorption bands along with higher intensity was observed in the Ce/Al-$SiO_2$ materials prepared at higher temperatures. In general, the band of UV absorption depends on not only the structure but also the dispersibility of the metal species. Since the Ce/Al-$SiO_2$ materials prepared at higher temperatures tended to have higher Ce loadings as shown in the

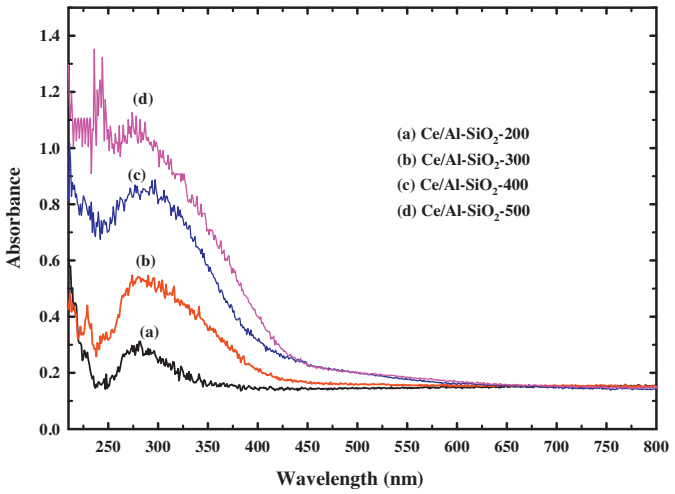


**Fig. 5.** UV–vis spectra of the washed Ce/Al-$SiO_2$ samples.

ICP-MS results (Table 1), the more Ce loadings resulted in the red shift and higher intensity in the absorption band, which may suggest the presence of more polymeric $CeO_2$ cluster species and the decreased dispersibility of the Ce species at higher Ce loadings of the Ce/Al-$SiO_2$ samples.

### 3.1.4. Formation mechanism

The possible pathway of formation of Ce/Al-$SiO_2$ microspheres through salt-templated aerosol process is illustrated in Fig. 6. In this work, sodium silicate solution extracted from the industrial waste silicate is firstly acidified with the aid of nitric acid to form activated silica sol, and the soluble $NaNO_3$ crystallites are in situ formed during the acidification process at the same time. Subsequently, aluminum and cerium nitrate are added as the metal precursors. When the precursor solution is aerosolized and heated, the droplets underwent rapid water evaporation; meanwhile, the silica oligomers, alumina oligomers and ceria oligomers can cross-link with each other through Si—O—metal bonds. During the heating process, as the aerosol processing temperature was higher, more polymeric metal clusters were formed in the resulting Ce/Al-$SiO_2$ sample, as confirmed by the ICP-MS and UV–vis results. On the other hand, the rapid evaporation of water also led to the solidification of the $NaNO_3$ salt, which can act as a template matrix to support the formation of porous structure. Finally, bimetallic Ce/Al catalysts supported on mesoporous $SiO_2$ microspheres are produced after the removal of $NaNO_3$ salts by water washing. For Ce/Al-$SiO_2$ sample prepared at 200 °C, the incomplete thermal decomposition of metal nitrates may result in the formation of hollow and fractured particles. Thus, it can conclude that mesoporous Ce/Al-$SiO_2$ microspheres can be facilely prepared using sodium silicate solution extracted from industrial waste silicates as the silicon precursor via an in situ salt-templated aerosol route.

The production yield and the silicon recovery yield were summarized in Table 1. The production yield was determined by the weight ratios in the precursor contents and the washed Ce/Al-$SiO_2$ samples, while the silicon recovery yield was determined by the weight ratio between silica contents in the as-prepared Ce/Al-$SiO_2$ and the silicon contents in the washed Ce/Al-$SiO_2$. It is noted that part of silica was removed during the water washing process. The increase in aerosol-spraying temperature resulted in both higher production yield and silicon recovery yield. This is probably due to that the increasing aerosol-spraying temperature could accelerate the thermal decomposition of metal nitrate precursors and solidification process of silica oligomers, resulting in higher production yield and silicon recovery yield.

### 3.1.5. Total acidity measurement

The $NH_3$-TPD was performed to investigate the number and strength of the acid sites in the Ce/Al-$SiO_2$ catalysts. As evident in Fig. 7, all washed catalysts present broad desorption processes within the temperature range of 50–900 °C, indicating a wide distribution of the surface acid strength. The total amounts of $NH_3$ desorbed from the catalysts are listed in Table 2, and the total acidity is found to decrease in the following order: Ce/Al-$SiO_2$-300 > Ce/Al-$SiO_2$-200 > Ce/Al-$SiO_2$-400 > Ce/Al-$SiO_2$-500. In general, the introduction of Ce and Al species in the silica framework both contributed to the surface acidity. Taking into account of the ICP-MS and $NH_3$-TPD results, it may

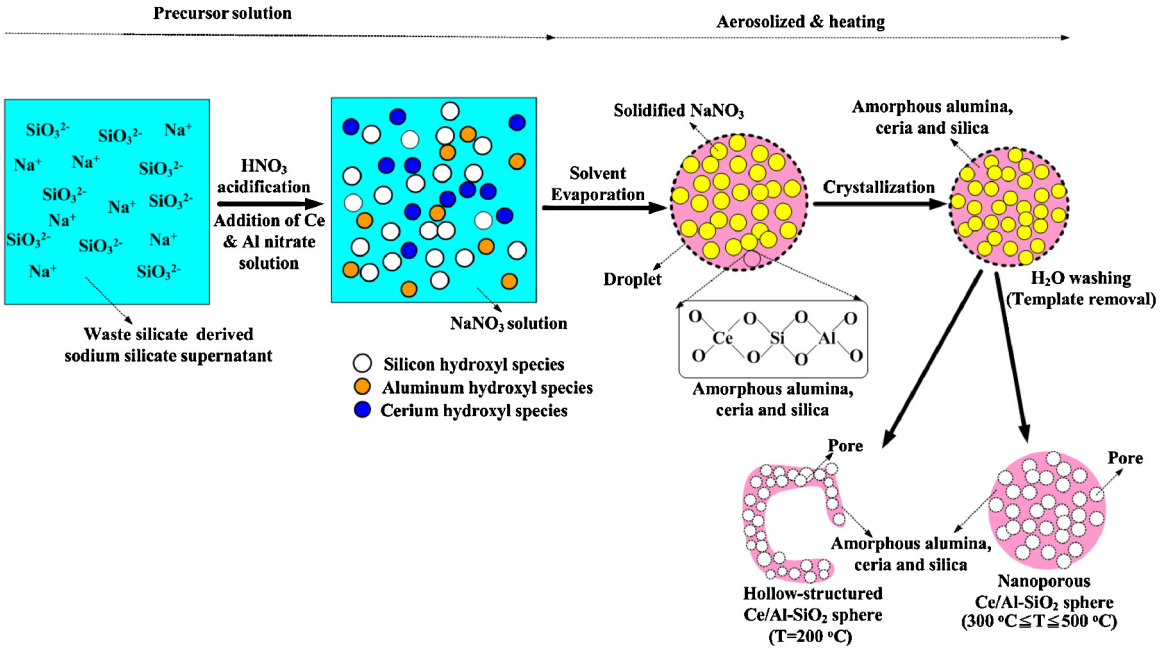


**Fig. 6.** A plausible formation mechanism of the mesoporous Ce/Al-$SiO_2$ microspheres.

**Table 2**
$H_2$ consumption, acidic properties and catalytic activities of the Ce/Al-$SiO_2$ catalysts.

| Catalysts | $H_2$ consumption (mmol $H_2$ $g^{-1}$) | Total acidity (mmol $NH_3$ $g^{-1}$) | Acid sites (%) | | | $T_{50}$ (°C) | $T_{90}$ (°C) |
|---|---|---|---|---|---|---|---|
| | | | Weak | Medium | Strong | | |
| Ce/Al-$SiO_2$-200 | 0.10 | 3.39 | 2.23 | 1.16 | – | 192 | 300 |
| Ce/Al-$SiO_2$-300 | 0.77 | 3.74 | 2.77 | 0.97 | – | 116 | 165 |
| Ce/Al-$SiO_2$-400 | 0.63 | 2.92 | 1.90 | 0.96 | 0.06 | 147 | 216 |
| Ce/Al-$SiO_2$-500 | 0.34 | 1.95 | 0.93 | 0.76 | 0.26 | 188 | 237 |
| Ce/Al-MSP | 0.71 | 3.75 | 2.75 | 0.86 | 0.14 | 115 | 175 |

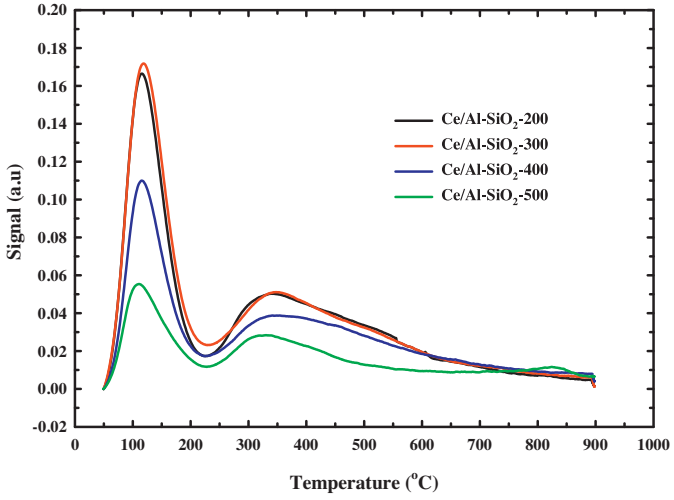


**Fig. 7.** $NH_3$-TPD profiles of the Ce/Al-$SiO_2$ and Ce/Al-MSPs catalysts.

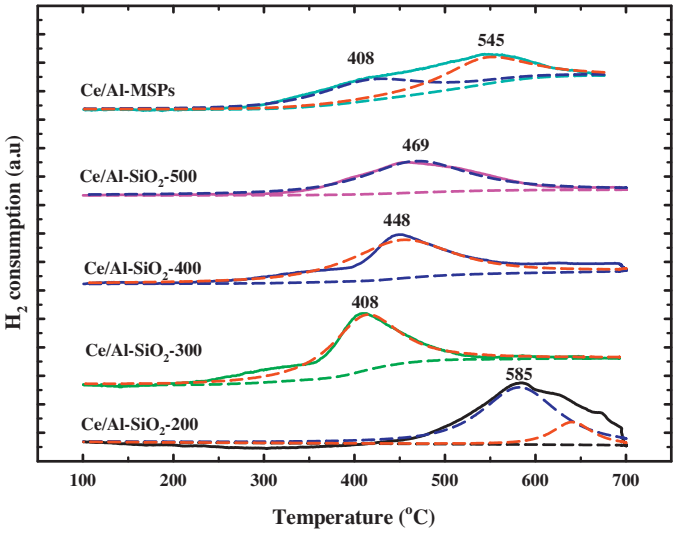


**Fig. 8.** $H_2$-TPR profiles of the Ce/Al-$SiO_2$ and Ce/Al-MSPs catalysts.

deduce that the acidity of the catalyst is probably influenced by the Ce content, since all Ce/Al-$SiO_2$ catalysts exhibited comparable Al content. It is observed that the total acidity is increased as Ce content increases from 0.3% (Ce/Al-$SiO_2$-200) to 1.73% (Ce/Al-$SiO_2$-300). Similarly, Kalita et al. [55] found the simultaneous introduction of Al and Ce species into silica network showed an enhanced acidity compared with Al-MCM-41, since the presence of Ce species can create additional Bronsted and Lewis acid sites. However, when the Ce loading is further increased, subsequent reduction in overall acidity is observed for Ce/Al-$SiO_2$-400 and Ce/Al-$SiO_2$-500, respectively. This could be ascribed to the partial blocking of the acid sites due to the formation of larger oxide clusters at higher Ce loadings.

### 3.1.6. Redox properties

The surface redox properties of Ce/Al-$SiO_2$ catalysts studied by the $H_2$-TPR measurement are displayed in Fig. 8, and the amounts of hydrogen consumption of all catalysts are summarized in Table 2. One sharp peak at ca. 408 °C is observed on Ce/Al-$SiO_2$-300. By analogy with previous studies on the reducibility of Ce-containing mesoporous materials [28,56], the peak is attributed to the reduction of dispersed tetrahedral coordinated cerium species. In the samples with higher Ce content (Ce/Al-$SiO_2$-400 and Ce/Al-$SiO_2$-500), the main peak shifted to 448 °C and 469 °C, respectively. The progressive shift of the maximum of the $H_2$ consumption peak to higher temperatures may suggest a progressive formation of less reducible highly polymeric $CeO_2$ cluster species. It has been reported that the redox property is strongly related to the physicochemical properties of the catalysts such as metal loading and dispersibility of the active metal phase [16,17]. Generally, catalyst with high degree of dispersion of metal components would favor stronger reducibility [11,18]. Since there are no crystalline materials revealed by the XRD and TEM analyses, Ce species are thought to present in highly dispersed form in Ce/Al-$SiO_2$ catalysts. As suggested by the increasing reduction temperatures of the $H_2$-TPR spectra and the red shift in the absorption band of the UV–vis spectra, the more Ce loadings, the more aggregated polymeric $CeO_2$ cluster species were formed, which may result in a poorer metallic dispersion and lower reducibility.

On the other hand, the Ce/Al-$SiO_2$-200 sample which exhibited the lowest Ce content showed a highest reduction temperature at 585 °C among all samples, suggesting the presence of more hardly reducible Ce species over other samples. In the previous works on metal species supported on mesoporous silica materials [57–59], it is found that metal species with relatively lower content, which mainly present as isolated ions strongly interacting with the support, required higher temperature to be reduced than those on the surface with a moderate metal loadings. Based on the above review, it can be proposed that the peak at 585 °C in Ce/Al-$SiO_2$-200 sample may be originated from the highly dispersed tetrahedral coordinated cerium species, which exhibited a strong interaction with the silica support. As demonstrated by the UV–vis result, Ce species are mainly presented as isolated cerium silicates in Ce/Al-$SiO_2$-200, which may result in too strong interaction with the support, and thus had a negative effect on its reducibility.

Moreover, it is interesting to observe that Ce/Al-MSP, which was synthesized with the aid of surfactant templates, showed two reduction peaks at 408 °C and 545 °C, which could be corresponded to the presence of dispersed tetrahedral cerium species and polymeric $CeO_2$ cluster species, respectively [28,56]. The emerging peak at 545 °C within Ce/Al-MSP may suggest the formation of less-reducible and highly polymeric cerium species. This phenomenon is probably related to the sintering effect since Ce/Al-MSP was calcined at 550 °C in order to completely remove the organic surfactants.

The surface reducibility of the catalysts has been demonstrated to be crucial for the heterogeneous catalytic reactions, since the

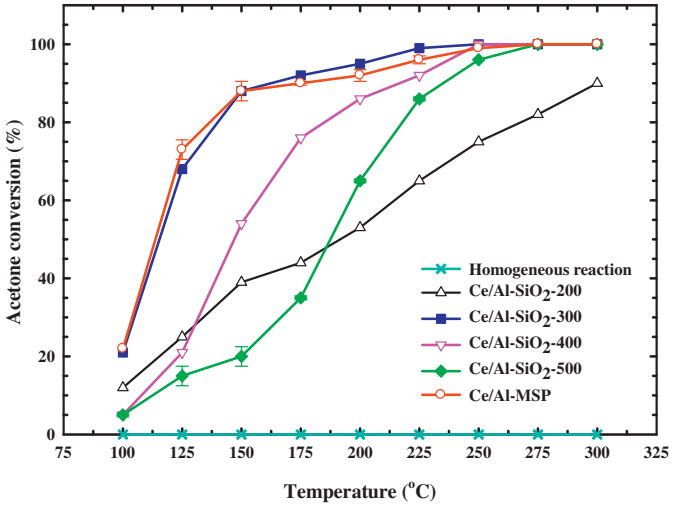


**Fig. 9.** Acetone conversion over the Ce/Al-$SiO_2$ and Ce/Al-MSPs catalysts.

reactions mainly take place on the catalyst surface. Hu et al. [60] showed that CuO-$CeO_2$ mixed oxides with lower $H_2$ consumption onset temperature presented higher catalytic activity in the oxidation of benzene. Chen et al. [15] found that the facile reduction feature of supported $CeO_2$ catalysts implied the easy activation for phenol oxidation. It is clear that high surface reducibility favors high catalytic activity since the reduction of reactive surface species frequently occurred at relatively lower temperatures. Moreover, as observed in Table 2, Ce/Al-$SiO_2$-300 consumed the highest amount of $H_2$ among all catalysts, indicating that there were more $H_2$-reducible Ce species in Ce/Al-$SiO_2$-300. Since $H_2$ consumption equates to oxidation of $H_2$ molecules, it may conclude that Ce/Al-$SiO_2$-300 has the highest oxidizing ability, while Ce/Al-$SiO_2$-200 has the poorest oxidizing ability.

### 3.2. Catalytic performance

In the blank experiment (in the absence of any catalyst), no conversion of acetone was detected below 300 °C under the conditions of acetone concentration = 1000 ppm and the GHSV = 15,000 $h^{-1}$, indicating that the homogeneous reaction of acetone was negligible under the adopted conditions. Fig. 9 shows the conversion of acetone as a function of the reaction temperature over Ce/Al-$SiO_2$ catalysts prepared at different aerosol-spraying temperatures. It can be seen that the acetone conversion increased gradually with the rise in reaction temperature and acetone was completely oxidized over all catalysts below 300 °C except Ce/Al-$SiO_2$-200. Under the reaction conditions, carbon dioxide was found to be the major carbonaceous product, which may be due to that acetone is simply structured organic compound.

The activities of the catalysts are evaluated by $T_{50}$ and $T_{90}$, corresponded to the temperature at 50% and 90% of acetone conversion, as summarized in Table 2. There are many parameters determining the VOCs oxidation efficiency, such as support textural property, surface reducibility and acidity of the supported catalyst [61,62]. Many researchers have reported the catalytic activity of supported catalysts for the VOCs oxidation is highly dependent on the surface reducibility of the catalysts [62–64]. It is observed that the order of acetone oxidation activity perfectly correlated with sequence of the catalysts as a function of surface reducibility (Ce/Al-$SiO_2$-300 ≈ Ce/Al-MSP > Ce/Al-$SiO_2$-400 > Ce/Al-$SiO_2$-500 > Ce/Al-$SiO_2$-200) as revealed by the $H_2$-TPR investigations. This points out that the surface reducibility on the catalysts, which is the presence of relatively accessible mobile oxygen species via facile reduction of $Ce^{4+} \rightarrow Ce^{3+}$ at low temperatures, is one of the main factors in the determination of catalytic performance. Noticeably, Ce/Al-$SiO_2$-200 was better than at lower temperatures (100–180 °C) but inferior above 185 °C to Ce/Al-$SiO_2$-500 in catalytic performance. Taking into account that Ce/Al-$SiO_2$-200 presented relatively higher acidity (3.33 mmol $NH_3$ $g^{-1}$) than that of Ce/Al-$SiO_2$-500 (1.95 mmol $NH_3$ $g^{-1}$), it may deduce that the surface acidity could also play a significant role in the reaction scheme, especially at lower temperatures. In fact, the key role of surface acidity in the oxidation of hydrocarbons has been demonstrated previously [65–68]. Wang and Bai [43] investigated the catalytic oxidation of acetone over Ce-MSP, Al-MSP and Ce/Al-MSP catalysts at temperature range of 150–350 °C. They found that Ce was the active metal for effective acetone removal, especially at relatively higher temperatures (>250 °C); while the co-presence of Ce and Al in MSP support resulted in a considerable increase in the total acidity, which is beneficial for enhancing the acetone removal at low temperatures (<200 °C). In this case, the high activity of Ce/Al-$SiO_2$-300 could be also related to its high acidity. On the other hand, although Ce/Al-$SiO_2$-200 presented a relatively larger number of acid sites (3.33 mmol $NH_3$ $g^{-1}$) than that of Ce/Al-$SiO_2$-400 (2.92 mmol $NH_3$ $g^{-1}$), its lowest surface reducibility resulted in a higher reaction temperature.

It is generally accepted that high-efficient supported catalyst often resulted from a large active surface area (small particle size) [61,69]. As observed in Tables 1 and 2, however, there is no relationship between $S_{BET}$, $V_{pore}$ and acetone oxidation. The results revealed that $S_{BET}$ and $V_{pore}$ are minor factors determining the catalytic performance. Interestingly, it is worth noting that Ce/Al-$SiO_2$-300 showed comparable reactivity to Ce/Al-MSP in the catalytic performance, even though the former catalyst presented much lower surface area and pore volume (681 $m^2$/g, 0.4 $cm^3$/g) than those of the latter one (917 $m^2$/g, 0.71 $cm^3$/g), as revealed in Table 1. Furthermore, Ce/Al-MSP is mainly composed of uniform and well-ordered mesostructure, which is beneficial for the rapid transfer of acetone molecules to the accessible active sites and facilitates the acetone oxidation process. However, the Ce/Al-MSP has fewer amounts of easily reducible cerium species and its reducibility is weaker than that of Ce/Al-$SiO_2$-300 as indicated previously from the $H_2$-TPR analysis. As a result, these two catalysts have a similar performance and it may suggest that both the surface redox property and the uniformity of the pore structure of the supported catalyst have significant impacts on catalytic performance. On the other hand, compared with other Ce/Al-$SiO_2$ materials, Ce/Al-$SiO_2$-300 displays a better pore uniformity, as shown in Fig. 3(b), which might provide more accessible active sites to the acetone molecules and benefit in acetone oxidation process. For Ce/Al-$SiO_2$-200 sample, its open-hollow structure with nanoporous shell might allow the acetone molecules access more easily to the active sites; however, its lowest surface redox property resulted in a higher reaction temperature. Considering the aforementioned results, it can be deduced that surface reducibility, catalyst acidity and pore structure have cumulative effects on acetone oxidation.

It is widely accepted that the oxidation of hydrocarbons over metal-loaded acid catalysts occurred through the adsorption of the hydrocarbon on acid sites and of the oxygen on active metal sites. Thus, it may deduce that the oxidation of acetone would be initiated by the adsorption of acetone on acid sites. Subsequently, the adsorbed molecules could be attacked by the mobile oxygen species from the solid solution via Mars-van Krevelen mechanism. This mechanism could be described in the following way:

$$\text{Acetone}_{(g)} + \ll \text{acidsites} \gg \rightarrow \text{acetone}_{(ads)} \quad (3)$$

$$\ll \square \gg + 1/2O_{2(g)} \rightarrow \ll O \gg \quad (4)$$

**Table 3**
Summary of various catalysts for acetone oxidation.

| Catalyst [Ref.] | Conditions (GHSV: $h^{-1}$, conc.: ppm) | Activity | |
|---|---|---|---|
| | | $T_{50}$ | $T_{90}$ |
| $LaCoO_3$ [70] | 14,100 $h^{-1}$, 1000 ppm | 222 | 244 |
| $LaMnO_3$ [70] | 14,100 $h^{-1}$, 1000 ppm | 203 | 224 |
| $Cu_{0.13}Ce_{0.87}O_y$ [71] | 15,000 $h^{-1}$, 1000 ppm | 200 | 223 |
| Ce-MSP [33] | 15,000 $h^{-1}$, 1000 ppm | 200 | 250 |
| Mn-MSP [33] | 15,000 $h^{-1}$, 1000 ppm | 230 | 289 |
| Ce/Al-MSP [42] | 15,000 $h^{-1}$, 1000 ppm | 115 | 175 |
| Ce/Al-$SiO_2$-300 (this study) | 15,000 $h^{-1}$, 1000 ppm | 116 | 165 |

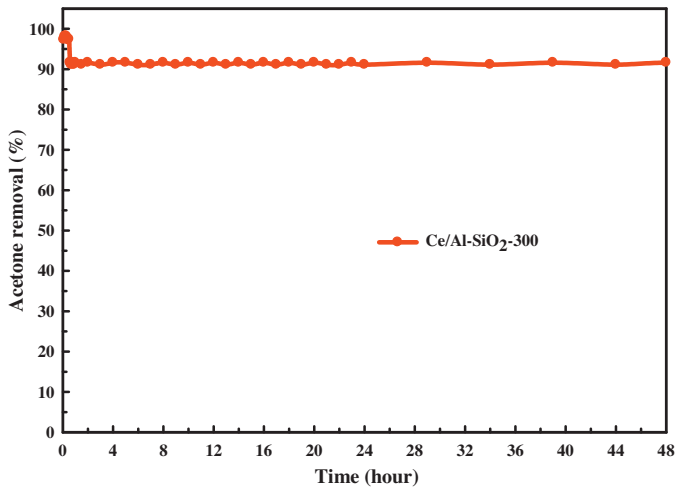


**Fig. 10.** Acetone conversion as a function of time-on-stream over Ce/Al-$SiO_2$-300 catalysts. Temperature: 225 °C, GHSV: 15,000 $h^{-1}$, acetone: 1000 ppm.

$$\text{Acetone}_{(ads)} + \ll O \gg \rightarrow CO_{2(g)} + H_2O_{(g)} + \ll \text{acidsites} \gg + \ll \square \gg \quad (5)$$

where ≪□≫ and ≪O≫ represents the oxygen vacancy and the mobile oxygen species, respectively. Taking together the characterization and catalytic oxidation results, it is therefore reasonable to suggest that the oxidation of acetone might be a demanding reaction that requires the adequate combination of surface redox property and acidity. The surface acid sites served as active sites for adsorption at low temperatures, which are beneficial for the oxidation of acetone. And the adsorption role might decrease, while the surface reducibility appears to play a more important role than acidity does with increasing the reaction temperatures.

The catalytic combustion of acetone has been studied over various catalysts during past years. One can see in Table 3 that most of the oxidation temperatures for 90% acetone conversion are higher than 200 °C, which are obviously higher than that of the Ce/Al-$SiO_2$-300 catalyst under similar conditions. Fig. 10 depicts the time-on-stream test over Ce/Al-$SiO_2$-300 to assess its long-term stability under conditions of 1000 ppmv acetone at a temperature of $T_{100}$ (225 °C). It was found that acetone conversion over Ce/Al-$SiO_2$-300 catalyst was stable at 92% after 48 h of operation time. The above results clearly suggest that the prepared Ce/Al-$SiO_2$-300 material in the current study might be considered as a potential catalyst for efficient VOCs oxidation.

## 4. Conclusions

Through a rapid and single-step process, bimetallic Ce/Al catalysts supported on mesoporous silica could be facilely fabricated. Due to the utilization of industrial waste silicate as the silicon precursor via a salt-templated aerosol process, the fabrication of mesoporous metal-$SiO_2$ microspheres is demonstrated to be scalable and cost-effective. The catalytic behavior of Ce/Al-$SiO_2$ catalyst was further studied in catalytic oxidation of acetone at temperature range of 100–300 °C. The results clearly showed that the oxidation of acetone is mainly associated with the surface redox property and the acidity of the catalyst. Based on favorable properties including high surface acidity and strong surface reducibility, Ce/Al-$SiO_2$-300 was demonstrated to be the most active catalyst among all samples. To date, there have been numerous reports regarding the reuse of a variety of waste silicas (e.g. rice husk, coal fly ash and power plant bottom ash) as the alternative silica resources; therefore, the proposed method may provide an excellent opportunity to prepare the mesoporous metal-$SiO_2$ catalysts economically on an industrial scale for a wide range of environmental protection applications.

## Acknowledgment

The authors gratefully acknowledge the financial support from the National Science Council of the Republic of China through grant No.: NSC 98-2221-E-009-023-MY3.

## Appendix A. Supplementary data

Supplementary data associated with this article can be found, in the online version, at http://dx.doi.org/10.1016/j.apcatb.2013.11.026.

## References

[1] F.I. Khan, A. Kr Ghoshal, J. Loss Prev. Process Ind. 13 (2000) 527–545.
[2] J.J. Spivey, Ind. Eng. Chem. Res. 26 (1987) 2165–2180.
[3] Q.-H. Xia, K. Hidajat, S. Kawi, Catal. Today 68 (2001) 255–262.
[4] L.F. Liotta, Appl. Catal. B: Environ. 100 (2010) 403–412.
[5] J. Zhu, T. Wang, X. Xu, P. Xiao, J. Li, Appl. Catal. B: Environ. 130–131 (2013) 197–217.
[6] M.T. Bore, M.P. Mokhonoana, T.L. Ward, N.J. Coville, A.K. Datye, Microporous Mesoporous Mater. 95 (2006) 118–125.
[7] E. Rezaei, J. Soltan, N. Chen, Appl. Catal. B: Environ. 136–137 (2013) 239–247.
[8] S.M. Saqer, D.I. Kondarides, X.E. Verykios, Appl. Catal. B: Environ. 103 (2011) 275–286.
[9] L.M. Gandía, M.A. Vicente, A. Gil, Appl. Catal. B: Environ. 38 (2002) 295–307.
[10] Á. Szegedi, M. Popova, A. Dimitrova, Z. Cherkezova-Zheleva, I. Mitov, Microporous Mesoporous Mater. 136 (2010) 106–114.
[11] B. de Rivas, C. Sampedro, R. López-Fonseca, M.Á. Gutiérrez-Ortiz, J.I. Gutiérrez-Ortiz, Appl. Catal. A: Gen. 417–418 (2012) 93–101.
[12] X. Zhang, S. Liu, H. Tong, G. Yong, Appl. Catal. B: Environ. 127 (2012) 105–111.
[13] T. Tabakova, D. Dimitrov, M. Manzoli, F. Vindigni, P. Petrova, L. Ilieva, R. Zanella, K. Ivanov, Catal. Commun. 35 (2013) 51–58.
[14] C.-H. Wang, S.-S. Lin, Appl. Catal. A: Gen. 268 (2004) 227–233.
[15] I.-P. Chen, S.-S. Lin, C.-H. Wang, L. Chang, J.-S. Chang, Appl. Catal. B: Environ. 50 (2004) 49–58.
[16] Q. Huang, X. Xue, R. Zhou, J. Hazard. Mater. 183 (2010) 694–700.
[17] Q. Huang, X. Xue, R. Zhou, J. Mol. Catal. A: Chem. 331 (2010) 130–136.
[18] B. de Rivas, C. Sampedro, E.V. Ramos-Fernández, R. López-Fonseca, J. Gascon, M. Makkee, J.I. Gutiérrez-Ortiz, Appl. Catal. A: Gen. 456 (2013) 96–104.
[19] Á. Szegedi, M. Popova, K. Lázár, S. Klébert, E. Drotár, Microporous Mesoporous Mater. 177 (2013) 97–104.
[20] D. Zhao, J. Feng, Q. Huo, N. Melosh, G.H. Fredrickson, B.F. Chmelka, G.D. Stucky, Science 279 (1998) 548–552.
[21] C.T. Kresge, M.E. Leonowicz, W.J. Roth, J.C. Vartuli, J.S. Beck, Nature 359 (1992) 710–712.
[22] J.A. Schwarz, C. Contescu, A. Contescu, Chem. Rev. 95 (1995) 477–510.
[23] R.J. White, R. Luque, V.L. Budarin, J.H. Clark, D.J. Macquarrie, Chem. Soc. Rev. 38 (2009) 481–494.
[24] M. Jin, J.H. Kim, J.M. Kim, J.-K. Jeon, J. Jurng, G.-N. Bae, Y.-K. Park, Catal. Today 204 (2013) 108–113.
[25] W.B. Li, M. Zhuang, T.C. Xiao, M.L.H. Green, J. Phys. Chem. B 110 (2006) 21568–21571.
[26] Z. Mu, J.J. Li, M.H. Duan, Z.P. Hao, S.Z. Qiao, Catal. Commun. 9 (2008) 1874–1877.
[27] Z. Mu, J.J. Li, H. Tian, Z.P. Hao, S.Z. Qiao, Mater. Res. Bull. 43 (2008) 2599–2606.
[28] M. Popova, á. Szegedi, Z. Cherkezova-Zheleva, I. Mitov, N. Kostova, T. Tsoncheva, J. Hazard. Mater. 168 (2009) 226–232.
[29] Z. Qu, Y. Bu, Y. Qin, Y. Wang, Q. Fu, Chem. Eng. J. 209 (2012) 163–169.
[30] T. Tsoncheva, G. Issa, T. Blasco, M. Dimitrov, M. Popova, S. Hernández, D. Kovacheva, G. Atanasova, J.M.L. Nieto, Appl. Catal. A: Gen. 453 (2013) 1–12.
[31] W. Zhao, J. Cheng, L. Wang, J. Chu, J. Qu, Y. Liu, S. Li, H. Zhang, J. Wang, Z. Hao, T. Qi, Appl. Catal. B: Environ. 127 (2012) 246–254.

[32] Z. Mu, J.J. Li, Z.P. Hao, S.Z. Qiao, Microporous Mesoporous Mater. 113 (2008) 72–80.
[33] C. Wang, H. Bai, Ind. Eng. Chem. Res. 50 (2011) 3842–3848.
[34] W. Zhan, Y. Guo, Y. Wang, X. Liu, Y. Guo, Y. Wang, Z. Zhang, G. Lu, J. Phys. Chem. B 111 (2007) 12103–12110.
[35] M.N. Timofeeva, S.H. Jhung, Y.K. Hwang, D.K. Kim, V.N. Panchenko, M.S. Melgunov, Y.A. Chesalov, J.-S. Chang, Appl. Catal. A: Gen. 317 (2007) 1–10.
[36] Á. Szegedi, Z. Kónya, D. Méhn, E. Solymár, G. Pál-Borbély, Z.E. Horváth, L.P. Biró, I. Kiricsi, Appl. Catal. A: Gen. 272 (2004) 257–266.
[37] M. Popova, Á. Szegedi, P. Németh, N. Kostova, T. Tsoncheva, Catal. Commun. 10 (2008) 304–308.
[38] M. Karthik, L.-Y. Lin, H. Bai, Microporous Mesoporous Mater. 117 (2009) 153–160.
[39] T. Sen, J. Whittle, M. Howard, Chem. Commun. 48 (2012) 4232–4234.
[40] W.B. Li, M. Zhuang, J.X. Wang, Catal. Today 137 (2008) 340–344.
[41] L.-Y. Lin, H. Bai, Environ. Sci. Technol. 47 (2013) 4636–4643.
[42] L.-Y. Lin, J.-T. Kuo, H. Bai, J. Hazard. Mater. 192 (2011) 255–262.
[43] C.Y. Wang, H. Bai, Catal. Today 174 (2011) 70–78.
[44] C.-C. Ting, H.-Y. Wu, A. Palani, A.S.T. Chiang, H.-M. Kao, Microporous Mesoporous Mater. 116 (2008) 323–329.
[45] H.-H.G. Tsai, P.-J. Chiu, G.-L. Jheng, C.-C. Ting, Y.-C. Pan, H.-M. Kao, J. Colloid Interface Sci. 359 (2011) 86–94.
[46] X.S. Wu, F.Z. Wang, S. Nie, J.S. Liu, L. Yang, S.S. Jiang, Physica C: Supercond. 339 (2000) 129–136.
[47] J. Schlomach, M. Kind, J. Colloid Interface Sci. 277 (2004) 316–326.
[48] L.K.C. de Souza, J.J.R. Pardauil, J.R. Zamian, G.N. da Rocha Filho, C.M. Barrado, R.S. Angélica, C.E.F. da Costa, Powder Technol. 229 (2012) 1–6.
[49] V. Meynen, P. Cool, E.F. Vansant, Microporous Mesoporous Mater. 125 (2009) 170–223.
[50] M.D. Donohue, G.L. Aranovich, J. Colloid Interface Sci 205 (1998) 121–130.
[51] S.H. Kim, B.Y.H. Liu, M.R. Zachariah, Chem. Mater. 14 (2002) 2889–2899.
[52] A.I. Carrillo, E. Serrano, J.C. Serrano-Ruiz, R. Luque, J. Garcia-Martinez, Appl. Catal. A: Gen. 435–436 (2012) 1–9.
[53] A. Prabhu, L. Kumaresan, M. Palanichamy, V. Murugesan, Appl. Catal. A: Gen. 374 (2010) 11–17.
[54] A. Bensalem, J.C. Muller, F. Bozon-Verduraz, J. Chem. Soc., Faraday Trans. 88 (1992) 153–154.
[55] P. Kalita, N.M. Gupta, R. Kumar, J. Catal. 245 (2007) 338–347.
[56] G. Calleja, J. Aguado, A. Carrero, J. Moreno, Appl. Catal. A: Gen. 316 (2007) 22–31.
[57] Á. Szegedi, M. Popova, C. Minchev, J. Mater. Sci. 44 (2009) 6710–6716.
[58] Á. Szegedi, G. Pál-Borbély, K. Lázár, React. Kinet. Catal. Lett. 74 (2001) 277–287.
[59] B. Solsona, M. Pérez-Cabero, I. Vázquez, A. Dejoz, T. García, J. Álvarez-Rodríguez, J. El-Haskouri, D. Beltrán, P. Amorós, Chem. Eng. J. 187 (2012) 391–400.
[60] C. Hu, Q. Zhu, Z. Jiang, Y. Zhang, Y. Wang, Microporous Mesoporous Mater. 113 (2008) 427–434.
[61] C. He, Q. Li, P. Li, Y. Wang, X. Zhang, J. Cheng, Z. Hao, Chem. Eng. J. 162 (2010) 901–909.
[62] C. He, J. Li, P. Li, J. Cheng, Z. Hao, Z.-P. Xu, Appl. Catal. B: Environ. 96 (2010) 466–475.
[63] C. He, L. Xu, L. Yue, Y. Chen, J. Chen, Z. Hao, Ind. Eng. Chem. Res. 51 (2012) 7211–7222.
[64] Z. Qu, Y. Bu, Y. Qin, Y. Wang, Q. Fu, Appl. Catal. B: Environ. 132–133 (2013) 353–362.
[65] N. Burgos, M. Paulis, M. Mirari Antxustegi, M. Montes, Appl. Catal. B: Environ. 38 (2002) 251–258.
[66] J.R. González-Velasco, R. López-Fonseca, A. Aranzabal, J.I. Gutiérrez-Ortiz, P. Steltenpohl, Appl. Catal. B: Environ. 24 (2000) 233–242.
[67] S. Chatterjee, H.L. Greene, J. Catal. 130 (1991) 76–85.
[68] S. Scirè, S. Minicò, C. Crisafulli, Appl. Catal. B: Environ. 45 (2003) 117–125.
[69] C. He, F. Zhang, L. Yue, X. Shang, J. Chen, Z. Hao, Appl. Catal. B: Environ. 111–112 (2012) 46–57.
[70] R. Spinicci, M. Faticanti, P. Marini, S. De Rossi, P. Porta, J. Mol. Catal. A: Chem. 197 (2003) 147–155.
[71] C. Hu, Q. Zhu, Z. Jiang, L. Chen, R. Wu, Chem. Eng. J. 152 (2009) 583–590.